IOP Conf. Series: Journal of Physics: Conf. Series **827** (2017) 012006 doi:10.1088/1742-6596/827/1/012006

Magnetic phase diagram of FeO at high pressure

Peng Zhang[1], R. E. Cohen[2], K. Haule[3]

1. Department of applied Physics, Xi'An Jiaotong university, Xi'An, China
2. Carnegie Institution of Washington, Washington D.C. USA
3. Department of Physics, Rutgers university, Piscataway, New Jersey, USA

E-mail: zpantz@xjtu.edu.cn

Abstract. FeO is an insulator with anti-ferromagnetic (AFM) spin ordering at ambient pressure. At increased external pressure, the Néel temperature of FeO first increases at the pressure below 40 GPa. Experiments predict that the AFM ordering will collapse above 80 GPa, but the mechanism of the high pressure magnetic collapse is still unknown. Using the combination of density functional theory and dynamical mean-field theory (DFT+DMFT), the nature of the magnetic collapse of FeO is examined and its magnetic phase diagram up to 180 GPa is discussed.

1. Introduction

The electrical and magnetic properties of FeO at high pressure attracts long lasting attention. FeO is the endmember to magnesiowüstite, the second most abundant materials in Earth's mantle. FeO has cubic rock salt structure (B1) at ambient pressure [1]. As external pressure is increased, it first transferred to rhombohedrally distorted (rB1) structure at about 17 GPa and room temperature [2, 3], next to the B8 structure as pressure is further increased [4, 5, 6, 7]. At ambient condition, FeO is an insulator. At high pressure and temperature, it has been proved both theoretically and experimentally there is an insulator to metal transition [8]. At ambient pressure and below 200 K [9], the magnetic moments of iron in FeO ordered ferromagnetically in planes perpendicular to [111] direction, but ordered antiferromagnetically between adjacent planes. As pressure is increased, the Néel temperature T_N increases linearly at pressure below 40 GPa [10, 11]. At higher pressure (P>80 GPa), the magnetism of FeO collapse, whereas the mechanism of such collapse is in debating. Mössbauer spectroscopy experiment by Pasternak et al. suggests such magnetic collapse results from high spin to low spin transition (HS-LS) in iron atom and FeO is in LS state at P>80 GPa [12]. But later x-ray emission spectroscopy experiment by Badro et al. suggests the collapse of magnetism comes from antiferromagnetism to paramagnetism (AFM-PM) transition [13]. Badro et al. proposed an arch shape Néel temperature as a function of pressure, which peaks at around 50 GPa and the magnetic moments is finite up to 143 GPa. Such discrepancy calls for a theoretical proof. But the known numerical researches on the Néel temperature of FeO are mostly limited to the low pressure region [14]. Due to underestimation of strong correlations among d-electrons of iron, DFT fails to give out insulate FeO at ambient condition [15]. Here we employ $state-of-the-art$ density functional theory and dynamical mean-field theory (DFT+DMFT) [16, 17] in investigation of magnetic phase diagram of stoichiometric FeO in cubic B1 structure up to 200 GPa and 1000 K. We found two coexisted magnetic transitions in FeO when external pressure is increased, the on-site

HS to LS crossover in iron atom and the ordering (AFM) to non-ordering (PM) transition of iron atoms. The HS state of iron atom crossover to LS state due to the electron transformation from e_g orbitals to t_{2g} orbitals and the pairing of these d-electrons.

2. Methods

In DFT+DMFT, the crystal problem is treated by solving the DFT equations, whereas the strong correlations are included by solving the DMFT equations. The outputs of DFT with self-energy correction are used to construct impurity levels and hybridization function for the DMFT calculation. After the DMFT iteration is converged, new charge density and self-energy are used for next DFT iteration. Our DFT+DMFT formalism iterates until full convergence of charge, chemical potential and self-energy. The WIEN2K package is used for the DFT part. Hybridization expansion continuous time quantum Monte Carlo (CTQMC) method [18, 19] is used as impurity solver of the DMFT equation to introduce all local electron-electron scattering. More details for the DFT+DMFT method is referenced to [16, 17]. The parameterized Hubbard U of 3d electrons is 8.0 eV, and the corresponding Hund's J is calculated from the Yukawa screening.

In the paramagnetic region, the bulk magnetic susceptibility has Curie-Weiss behavior $\chi_q^m \propto \frac{1}{T-T_N}$ as the temperature is decreasing, and diverges at the Néel temperature $T = T_N$. In order to derive the bulk magnetic susceptibility from magnetic susceptibility on the DMFT impurity site, we calculated the magnetic vertex function from Bethe-Salpeter equation, which connects the bulk magnetic susceptibility with the impurity magnetic susceptibility.

$$1/\chi^0_{m,i} - 1/\chi_{m,i} = \Gamma_m = 1/\chi^0_{m,q} - 1/\chi_{m,q} \tag{1}$$

in which i is impurity index, q is moment, m indicates the magnetic susceptibility. Due to numerical efficiency, we truncated number of Fermionic frequency in our CTQMC measurements of the impurity magnetic susceptibility and in derivation of bulk magnetic susceptibility. We use bare magnetic susceptibility in real frequency to recover the lost part due to truncation of Fermionic frequency.

3. Results

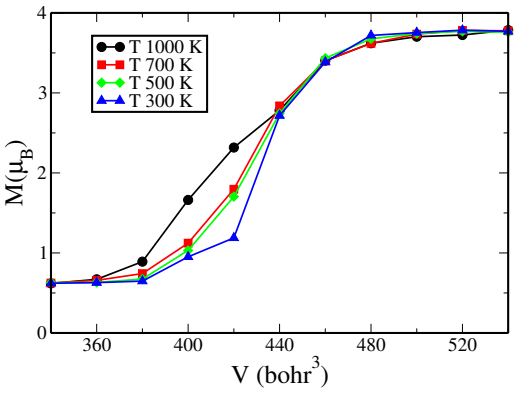

Figure 1: Magnetic moment of iron atom in FeO as a function of volume at temperature from 300 K to 1000 K. The magnetic moment of iron decreases as lattice volume is decreased, and the process of decrement is enhanced at lower temperature.

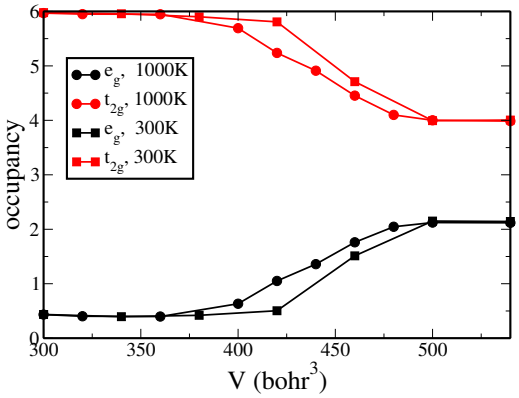

Figure 2: Electron occupancy on e_g and t_{2g} orbitals of iron atom in FeO at 300 K and 1000 K. As lattice volume is decreased, electrons on e_g orbitals transfer to t_{2g} orbitals. At lower temperature, the process of electron transfer is enhanced.

In Fig. 1, the magnetic moment $M = g\sqrt{\langle S_z^2 \rangle}$ of iron in FeO is plotted as a function of lattice volume at temperatures from 300 K to 1000 K. As volume is compressed, magnetic moment of FeO gradually decreases. When temperature is decreased, the magnetic moment versus volume curves get steeper in the region of decrement. The magnetic moment versus volume curves converge at T<300 K. It indicates there is HS-LS transition in FeO as lattice volume is decreased, and the HS-LS transition is a crossover. The magnetic moments and the corresponding HS-LS transition in transition metal compounds usually result from partitioning and pairing of their d-electrons. This scenario is presented in Fig. 2. At V=540 $bohr^3$, there are about 4 electrons on t_{2g} orbitals and about 2 electrons on e_g orbitals. In atomic electron configuration, 4 up spins and 2 down spins give out atomic magnetic moment of $4\mu_B$. As volume is decreased from 500 $bohr^3$ to 360 $bohr^3$, electrons on e_g orbitals gradually transfer to t_{2g} orbitals. At 300 $bohr^3$, there is no electrons on e_g orbitals. The pairing of all 6 electrons on t_{2g} orbitals leads to the LS state. The speed of electron transfer is enhanced as temperature is decreased. The electron transfer from e_g orbitals to t_{2g} orbitals results from shifts of density of state (DOS) from e_g orbitals to t_{2g} orbitals, as shown in Fig. 3. In Fig. 3a, there are finite DOS on both e_g orbitals and t_{2g} orbitals above and below the Fermi level. The Fermi level falls in the gaps of e_g orbitals and t_{2g} orbitals, which indicates FeO is both Mott insulator and charge transfer insulator. The insulator state of FeO in our numerical calculation at the ambient condition is consistent with experiment results. In contrast, although in Fig. 3b FeO is still an insulator at 300 $bohr^3$, the DOS of e_g orbitals is zero below the Fermi level and the DOS of t_{2g} is zero above the Fermi level. There is no DOS available on e_g orbitals for electrons to occupy. All d-electrons are pushed to t_{2g} orbitals. FeO is no longer a Mott insulator at 300 $bohr^3$.

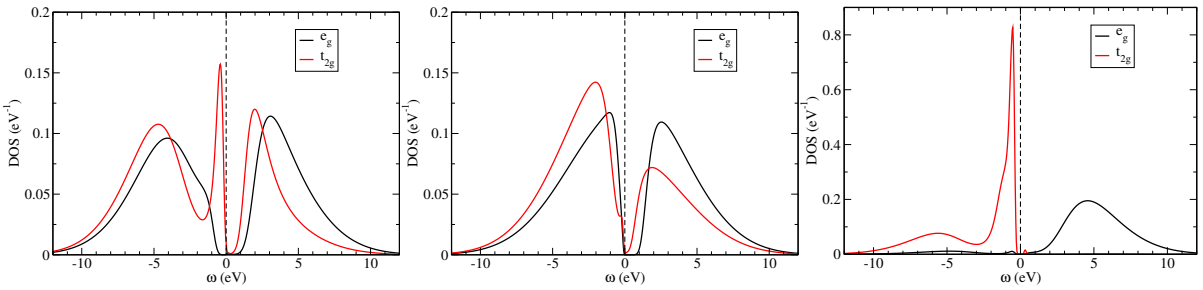

Figure 3: Density of states (DOS) on e_g and t_{2g} orbitals of iron atom in FeO at 300 K, (a) 540 $bohr^3$ (b) 420 $bohr^3$ (c) 300 $bohr^3$. As volume is decreased, DOS on e_g orbitals transfers to t_{2g} orbital, until at 300 $bohr^3$ there is no DOS below the Fermi level on e_g orbitals. FeO is always an insulator at all volumes.

Inverse bulk magnetic susceptibility χ_m^{-1} at $q = (\pi, \pi, \pi)$ as a function of temperature at various volumes in the paramagnetic region is plotted in Fig. 4. Since the bulk magnetic susceptibility $\chi_m(q = (\pi, \pi, \pi), T)$ behaves as $1/(T - T_N)$ in the paramagnetic region, which diverges at $T = T_N$, inverse of the bulk magnetic susceptibility $\chi_m^{-1}(q = (\pi, \pi, \pi), T)$ is linear with temperature. When we extrapolate the linear fit of $\chi_m^{-1}(q = (\pi, \pi, \pi), T)$ as a function of decreased temperature, the Néel temperature T_N is derived at the temperature where the linear fit crosses the temperature-axis. The derived Néel temperature at each volume is presented in legend of Fig. 4. The Néel temperature first increase as volume is compressed (or the pressure is increased); it peaks at 380 $bohr^3$ and then decrease at smaller volumes (or at higher pressures).

To summarize, we have find there are two magnetic transitions in FeO at increased pressure: a HS-LS transition as well as a AFM-PM transition. At above 80 GPa, the magnetic moment

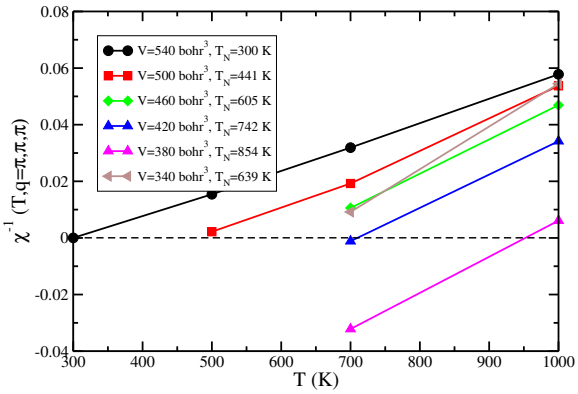

Figure 4: Inverse bulk magnetic susceptibility of FeO as a function of temperature at volumes from 540 $bohr^3$ to 300 $bohr^3$. The Nel temperature T_N is derived by linear extrapolation of $\chi^{-1}(T, q = (\pi, \pi, \pi))$ vs. T line to x-axis, where $T = T_N$. The corresponding Nel temperature T_N at each volume is presented in the legend.

of iron atom in FeO is nonzero. Our derived Néel temperature first increase then decrease with increased pressure. These results are consistent with previous experiment on FeO [20] and theoretical [21, 22] results of magnesiowstite.

3.1. Acknowledgments
This research used the NSF Extreme Science and Engineering Discovery Environment (XSEDE) supercomputer Stampede as well as the supercomputer Mw in Geophysical Laboratory, Carnegie Institution of Washington.

4. References

[1] Willis B T M and Rooksby H P 1953 *Acta Crystallogr.* **6** 827
[2] Zou G, Mao H K, Bell P M and Virgo D 1980 *Carnegie Inst. Washington Yearbook* **79**
[3] Yagi T, Suzuki T and Akimoto S 1985 *J. Geophys. Res.* **90** 8784
[4] Ozawa H, Hirose K, Tateno S, Sata N and Ohishi Y 2010 *Physics of the Earth and Planetary Interiors* **179** 157–163
[5] Fei Y and Mao H K 1994 *Science* **266** 1678
[6] Mazin I I, Fei Y, Downs R and Cohen R 1998 *Am. Mineral.* **83** 451
[7] Kondo T, Ohtani E, Hirao N, Yagi T and Kikegawa T 2004 *Phys. Earth Planet. Inter.* **201** 143–144
[8] Ohta K, Cohen R E, Hirose K, Haule K, Shimizu K and Ohishi Y 2012 *Phys. Rev. Lett.* **108** 026403
[9] McCammon C A 1992 *J. Magn. Magn. Mater.* **104** 1937–1938
[10] Nasu S, Kurimoto K, Nagatomo S, Endo S and Fujita F E 1986 *Hyperfine Interactions* **29** 1583
[11] Kantor I, Dubrovinsky L, Mccammon C, Dubrovinskaia N, Goncharenko I, Kantor A, Kuznetsov A and Crichton W 2007 *Phase Transitions* **80** 1151–1163
[12] Pasternak M P, Taylor R D, Jeanloz R, Li X, Nguyen J H and McCammon C A 1997 *Phys. Rev. Lett* **79** 5046
[13] Badro J, Struzhkin V V, Shu J, Hemley R J and Mao H 1999 *Phys. Rev. Lett.* **83** 4101
[14] Wan X, Yin Q and Savrosov S Y 2006 *Phys. Rev. Lett.* **97** 266403
[15] Cohen R E, Fei Y, Downs R, Mazin I I and Isaak D G 1998 **499** 27–40
[16] Kotliar G, Savrasov S Y, Haule K, Oudovenko V S, Parcollet O and Marianetti C A 2006 *Rev. Mod. Phys.* **78** 865
[17] Haule K, Yee C and Kim K 2010 *Phys. Rev. B* **81** 195107
[18] Werner P, Comanac A, de Medici L, Troyer M and Millis A J 2006 *Phys. Rev. Lett.* **97** 076405
[19] Haule K 2007 *Phys. Rev. B* **75** 155113
[20] Badro J, Fiquet G, Guyot F, Rueff J, Struzhkin V V, Vankó G and Monaco G 2003 *Science* **300** 789–791
[21] Tsuchiya T, Wentzcovitch R M, da Silva C R S and de Gironcoli S 2006 *Phys. Rev. Lett.* **96** 198501
[22] Holmström E and Stixrude L 2015 *Phys. Rev. Lett.* **114** 117202